X-913-74-209
PREPRINT
NASA TM X- 70721

INFORMATION CONTENT OF IRIS SPECTRA

JOHN C. PRICE

JUNE 1974

GSFC
GODDARD SPACE FLIGHT CENTER
GREENBELT, MARYLAND

INFORMATION CONTENT OF IRIS SPECTRA

John C. Price

June 1974

GODDARD SPACE FLIGHT CENTER

Greenbelt, Maryland

CONTENTS

ILLUSTRATIONS

INFORMATION CONTENT OF IRIS SPECTRA

John C. Price

Atmospheric and Hydrospheric Applications Division

ABSTRACT

Spectra from the satellite instrument IRIS (Infra Red Interferometer Spectrometer) were examined to find the number of independent variables needed to describe these broadband high spectral resolution data. The radiated power in the atmospheric window from 771 to 981 cm^{-1} was the first parameter chosen for fitting observed spectra. At succeeding levels of analysis the residual variability (observed spectrum - best fit spectrum) in an ensemble of observations was partitioned into spectral eigenvectors. The eigenvector describing the largest fraction of this variability was examined for a strong spectral signature; the power in the corresponding spectral band was then used as the next fitting parameter. The measured power in nine spectral intervals, when inserted in the spectral fitting functions, was adequate to describe most spectra to within the noise level of IRIS. Considerations of relative signal strength and scales of atmospheric variability suggest a combination sounder (multichannel-broad field of view) scanner (window channel-small field of view) as an efficient observing instrument.

INTRODUCTION

The Nimbus 4 satellite sensor called the IRIS (Infra Red Interferometer Spectrometer) (Nimbus IV Users Guide, 1970), (Hanel, et al., 1972) produced a large number of broadband (400-1600 cm^{-1}), high resolution (2.8 cm^{-1}) spectra from nadir views of the earth for a period of a year beginning in 1970. This study considers only the variability of these spectra. The spectral data may be used for atmospheric soundings of temperature, water vapor, ozone, for identification of cloud features, and for studies of surface temperature and surface composition. Incorporation of laboratory spectroscopic results into a radiative transfer program to predict the spectra is a major undertaking (Kunde and Maguire, 1974). The application of the observed spectra for practical purposes (e.g., temperature surroundings for meteorological prediction) requires, in addition, an inversion program to derive physical variables from the observed radiances. The purposes of the present study are much simpler: to discover how many independent pieces of information (variables) exist in the observed spectra, the regions of the spectrum in which these variables are strongest, and to determine realistic values for bandwidth and signal strength for optimum satellite sensing in the infrared.

The results described here permit the design of optimized satellite instruments by defining the number, spectral location and channel bandwidth for remote sensing in the spectral interval 400-1600 cm^{-1}. The knowledge of the number and locations of these bands should permit development of more efficient and more accurate inversion programs for defining the physical situation being observed.

Several limitations exist in this study due to the nature of the data. The first is that of instrument noise, which places a lower bound on signals which can be isolated, even using statistical processing to enhance these signals. A second source of difficulty arises from the existence of infrequent (generally 1-2 per thousand) faulty spectra which have slipped through the quality control filters in the original data reduction. These faulty spectra play the role of an additional noise source in the statistical data processing and also tend to place a lower limit on the strength of the signals which can be reliably isolated.

It is obvious that instrument noise and occasional faulty spectra tend to increase the total variability of the spectra, and hence to provide additional spurious signals. Physical considerations indicate that all spectral bands defined here do measure "true" variability in the earth-atmosphere system. It also appears that an instrument with better signal/noise is required to extend the number of signals very far beyond the nine reported here.

A final limitation is imposed by the variability inherent even in large data volumes, and the need to restrict computer usage to a reasonable level. The use of small data samples in determining fitting coefficients produces less than optimal results. Although one day's data consists of approximately 4000 spectra, a variation from one day's data to the next is noticeable. In all statistical programs for obtaining fitting coefficients we have used tapes representing 4 days of data distributed at roughly three month intervals through a year. This

represents 11-14000 spectra in each case. Data from different days were used for each run, so that the full variability of the data was sampled. However, larger samples would have yielded slightly more efficient fitting routines, at the cost of an increase in computer processing.

Section II describes in general terms the procedure used in carrying out the analysis. Questions arise which require decisions based on tradeoff between instrument capability, error propagation, and uncertainties due to finite data samples. The framework developed here may be modified to evaluate the capabilities of other satellite instruments, or to reflect a greater importance of certain of the tradeoff parameters.

In section III the mathematical model of analysis is described in detail. The results and conclusions are presented in section IV.

PROCEDURE

The procedure used here consists of obtaining a sequence of fitting functions which represent better and better approximations to the observed IRIS spectra. These approximations represent improvements in the sense that the root-mean-square difference in radiance between the observed and the fitted spectra gets smaller and smaller at each level of processing. In going from one level of approximation to the next, two operations must be carried out:

1. The total spectral variability remaining at the current level of processing is assessed by taking the difference between large numbers of

observed spectra and their respective best fit spectra. Each difference is treated as a vector of dimension 862 corresponding to the number of points resolved by the IRIS. This spectral variability is then partitioned into independent variables (eigenvectors) by means of a statistical analysis of an ensemble of difference vectors. Each of these spectral eigenvectors has a strong spectral signature in some frequency interval, plus a smaller signal throughout the rest of the IRIS spectral bandpass. Each eigenvector shows variability across the full spectral band 400 to 1600 cm^{-1} because of physical correlations (e.g., water vapor lines appear throughout the spectrum) or because of meteorological correlations (e.g., temperature and humidity are statistically related). Examination of the eigenvector describing the largest part of the variance leads to the choice of the next spectral band containing a strong spectral signature which will be used in obtaining an improved fit to the spectrum.

2. The integrated power of this spectral band is used in obtaining a one parameter fitting function for another larger ensemble of difference vectors. This fit consists of a polynomial series in the power in this spectral band, with coefficients adjusted for a best fit. At this point the approximation procedure has been improved in the sense that another spectral fit to the full spectrum has been defined. This fit reduces further the difference between observed spectra and their respective best fit spectra.

At each step a decision must be made on the width of the spectal band for sensing the relevant spectral signature. Generally widening the spectral bandpass means an increase in signal strength, with a resulting improvement in the signal to noise ratio. Values of instrument noise are produced as part of the routine data reduction for IRIS; a representative noise spectrum is shown in Figure 1. Although a wider bandwidth increases the signal to noise ratio, it also results in more interference (crosstalk) from variables which are strongest in other parts of the spectrum. For example, interference due to absorption lines of water vapor appears in almost all of the spectral bands. In most cases this tradeoff affects the choice of spectral bandwidths only slightly.

Another decision must be made which affects the order in which spectral bands are chosen. This is the choice of the normalization of difference vectors for the eigenvector analysis. In this study all spectral difference vectors $\delta S(\nu)$ were divided by a representative value of the instrument noise $N(\nu)$ so that intervals with higher instrument noise, particularly near $1600\,cm^{-1}$, do not contribute excessively to the spectral eigenvectors. A different choice of normalization would affect the order in which spectral intervals are chosen. For example if all radiances were converted to temperature at the start of the analysis the $1600\,cm^{-1}$ region of the spectrum would be greatly emphasized because temperature varies more rapidly with energy at this end of the spectrum.

Mathematical Methods

The choice of the initial spectral band for fitting the spectrum is largely arbitrary. Examination shows that all spectra have the shape of blackbody functions, with superimposed strong absorption bands (for very cold spectra: emission) corresponding to CO_2 at 600-750 cm^{-1} and O_3 at 1000-1100 cm^{-1}. The cleanest atmospheric window from 771 to 981 cm^{-1} was chosen as the spectral band for identifying the blackbody temperature which yields the envelope for the observed spectrum. This choice provides a signal with an ensemble mean value of approximately 15000 ergs-cm^{-2}-$ster^{-1}$-sec^{-1}, without much interference from other atmospheric variables such as CO_2, water vapor, etc. It was discovered after considerable computer processing that the narrower interval 820-981 cm^{-1} would have eliminated interference from the wing of the CO_2 absorption, but the analysis was not repeated because of the computer time involved. Other possible bands are 771 to 1250 cm^{-1}, with interference from O_3 and H_2O, and 400 to 1250 cm^{-1}, with additional interference from the strong CO_2 band centered at 667 cm^{-1}. The total spectral power from 400 to 1600 cm^{-1} also provides a logical first parameter, at the expense of treating all other variables as interference which must be subtracted out. Such overlapping measurements tend to enhance the effects of instrument noise and destabilize data analysis procedures.

Let P_1^i denote the power in ergs-cm^{-2}-$ster^{-1}$-sec^{-1} in the first spectral interval for the ith observed spectrum $S^i(\nu)$. Thus $P_1^i(\nu_1^o, \nu_1^f) = \int_{\nu_1^o}^{\nu_1^f} d\nu\, S^i(\nu)$

where $\nu_1^o = 771\,cm^{-1}$ and $\nu_1^f = 981\,cm^{-1}$ define the spectral band. Using the power in this first spectral interval P_1^i, an approximate fit $S_0^i(P_1^i, \nu)$ to the envelope of the spectrum is determined.

The spectrum envelope is essentially a blackbody curve with the effective temperature T^i identified from P_1^i, and with sections cut out from 580-760 cm^{-1} (CO_2), from 990-1070 cm^{-1} (O_3) and from 1230-1600 cm^{-1} (H_2O). Empirical coefficients determined from a large number of spectra ensure that the crude fit has the general shape of actual spectra. Figure 2 shows $S_0(\nu)$ for a representative value $P_1 = 14,300$ erg-cm^{-2}-$ster^{-1}$-sec^{-1}. This fit is then adjusted by a power series in $(T^i - 270^\circ)$ in order to yield a one parameter description of the IRIS spectra.

$$S_1^i(\nu) = S_o^i(T^i, \nu) + a(\nu) + b(\nu)(T^i - 270^\circ) + c(\nu)(T^i - 270)^2 + d(\nu)(T^i - 270^\circ)^3 \quad (1)$$

The constants a, b, c, d are determined by a statistical analysis using the observed spectra. The ensemble average (four days spectra) of the product of Equation 1 with $[1,\ T^i - 270^\circ,\ (T^i - 270^\circ)^2,\ (T^i - 270^\circ)^3]$ results in four simultaneous equations which may be solved for a-d, each as a function of ν. The resultant one parameter fit of the full spectrum is shown in Figures 3a-f for P_1 = 2300-32,300 erg-cm^{-2}-$ster^{-1}$-sec^{-1} at intervals of 6000. This range encompasses all but a very few of the IRIS spectra.

The procedure for obtaining higher order approximations is similar.

The first spectral fit S_1 provides a starting point for a scheme in which successive levels are obtained by mathematical induction. At the nth level the capability to fit spectra using n parameters is assumed. Each spectrum S^i from an ensemble may be approximated by a sum of fitting functions using these n parameters. Let δS^i_{n+1} be the difference between the actual spectrum and the fitted spectrum of order n, where i labels the member of the ensemble.

$$\delta S^i_{n+1} = S^i - \sum_{j=1}^{n} S^i_j$$

These spectral difference vectors show variability throughout the IRIS spectral bandpass 400 to 1600 cm^{-1}. The next task is to choose a spectral interval which contains most of this variability so that the power in this band may be used as the next fitting parameter. For this purpose statistical processing is essential. The observed spectra represent the total variability of the globe, including polar ice caps, vegetated land, deserts, oceans, and various cloud types and amounts. Large numbers of spectra (an ensemble) must be used in order to obtain representative results.

As described previously, the initial step in choosing regions of spectral variability is to divide each difference spectrum by a representative value of instrument noise $N(\nu)$. These vectors $V^i(\nu) = \delta S^i(\nu)/N(\nu)$ are used as input to the Gram-Schmidt procedure (Apostol, 1957) in order to obtain independent vectors representing the full variability in one day's data. During this procedure residual

vectors which are near the noise level are eliminated in order to keep the number of Gram-Schmidt vectors reasonably small. In addition as the analysis proceeded techniques for identifying and rejecting faulty spectra were developed. Typically one days data would produce 25 Gram-Schmidt vectors (the maximum permitted) at the early levels of approximation and 10-15 at the later stages.

These vectors E_ℓ are normalized in the usual fashion $E_\ell \cdot E_m \equiv \sum_{J_\nu=1}^{862} E_\ell(J_\nu)$ $E_m(J_\nu) = \delta_{\ell m}$, where $\delta_{\ell m}$ is the Kronecker delta. Next a second day's data is resolved into these vectors. Thus $V^i = \sum_{\ell=1}^{25} a^i_\ell E_\ell$, where the coefficient a^i_ℓ is given by $a^i_\ell = V^i \cdot E_\ell$. From a days worth of data the covariance matrix $A_{\ell m} = 1/N \sum_{i=1}^{N} a^i_\ell a^i_m$ is computed (Lawley and Maxwell, 1963). This convariance matrix is next reduced to diagonal form by application of a transformation matrix $B_{k\ell}$ composed of the eigenvectors of A. The magnitudes of the eigenvalues of A indicate the amount of the total variance explained with the first eigenvector usually accounting for 40-70% of the total variance. By using the transformation matrix the full spectral eigenvectors are reconstructed by $e_\ell = \sum_{k=1}^{25} B_{k\ell} E_k$.

At this point a plot of the first spectral eigenvector shows a large amplitude in one spectral interval, with minor variability in the rest of the IRIS bandpass. As described in section II a subjective decision is made as to the optimum spectral interval for detecting this spectral variation.

As already noted, despite the large number of spectra in one days data, approximately 4000, there is a noticeable variability in the eigenvector analysis

from one day to another. The computer time associated with subtracting off the spectral best fit, followed by the projection of the components E_ℓ, placed a limit on the sample sizes permitted. In addition, the Gram-Schmidt analysis tended to result in moderate amounts of noise in the spectral eigenvectors. Both defects were largely eliminated in the spectral fitting functions, which were obtained from much larger data samples. Figures 4a-h, showing the fitting functions at typical power values, are representative of the first of the successive eigenvectors.

It is now possible to define the next fitting function. The residual power in the n + 1 st spectral band (ν^o_{n+1} , ν^f_{n+1}) is computed by

$$\delta P^i_{n+1} = \int_{\nu^o_{n+1}}^{\nu^f_{n+1}} d\nu \, \delta S^i_{n+1} (\nu)$$

From an ensemble of such difference spectra and band power measurements the set of coefficients a_{n+1}, b_{n+1}, c_{n+1}, d_{n+1} (ν) is computed for the next spectral fit

$$S^i_{n+1} = a_{n+1} + b_{n+1} \delta P^i_{n+1} + c_{n+1} [\delta P^i_{n+1}]^2 + d_{n+1} [\delta P^i_{n+1}]^3 \qquad (2)$$

The coefficients are obtained by computing the ensemble mean of the product of Equation 2 with $[1, P^i_{n+1}, (P^i_{n+1})^2, (P^i_{n+1})^3]$. The resulting four equations permit a solution for a_{n+1}-d_{n+1} at each observed frequency. The inclusion of quadratic and cubic terms permits a more efficient description of the spectra by allowing the shape of the fitting functions to change as well as the amplitude.

The eight functions S_2-S_9 defined here fit the observed spectra better than the 25 eigenvectors (corresponding to a linear analysis) in the first partitioning of spectral variability. This completes the derivation of S_{n+1}, given S_1, S_2 - - S_n.

RESULTS

The procedures just described lead to the identification of nine spectral intervals which represent almost all of the variability of the observed spectra. Columns one and two of Table 1 list the band pass (ν_n^o , ν_n^f) of the respective bands. Column three lists the ensemble average values of the power (erg-cm^{-2} - ster^{-1}-sec^{-1}) observed in each of these channels. The variation of the power in the first channel represents the first parameter used in fitting the full spectrum. From the first entries of columns four and five the standard deviation of the first parameter is 5338 erg-cm^{-2} -ster^{-1} -sec^{-1} , representing approximately 35% variability in the received power. Succeeding entries in columns four and five are values for the residual variability in the channel after the fitting procedure is carried out using all previous parameters. The trend toward smaller numbers in column five indicates the decreasing amount of variability explained by each new parameter. The ninth spectral band represents an apparent exception to the trend. This variation did not appear until late in the analysis because of the combination of low total signal strength and the poor signal to noise of the IRIS instrument in this spectral region.

In Figures 4a-h the spectral fitting functions are plotted for a value of the power equal to plus one standard deviation of the observed variability. The first fitting function effectively removes the average values from all spectral intervals. Therefore the ensemble means of parameters 2-9 are essentially zero. Plots of the fitting functions at minus one standard deviation of the power closely resemble mirror reflections (about the abcissa) of Figures 4a-h. The dependence on δP_i^2 and δP_i^3, which changes the shape of fitting functions, shows up only for larger signal strengths - typically 2-3 standard deviations.

Only band number 6, associated with Q branch of the CO_2 absorption, is a narrow spectral feature. With this exception broad band measurements appear adequate to describe the spectrum in full detail, because the variability of fine spectral details is correlated with that of broad spectral features. At the level of sophistication of this analysis the high spectral resolution provides a desirable research capability but is not needed for meteorological purposes.

It must be emphasized that it is not possible to equate the variation in a particular spectral band with a single meteorological variable. The spectrum is the algebraic sum of the contributions from the 9 spectral features described here. Despite this fact it is possible to make a general identification of each of the spectral bands with known meteorological variables, as shown in column six.

Although band 7 appears to represent variability in the lower tropospheric temperature, the width of the derived fitting function also suggests a cloud effect. Curran (1972) has shown that thin clouds may cause a decrease in radiation in this spectral region. In addition a field of view effect was expected, with a warm surface partially covered by cold clouds showing different features from a middle cloud layer at an intermediate temperature. Although this field of view effect must occur (the IRIS field of view was 90 km in diameter) it is presumably correlated with other variability in the spectrum.

The analysis was terminated because the tenth spectral interval overlapped interval 1. This indicates that more care in developing the fitting procedure for the first spectral variable would have been appropriate. In addition occasional faulty spectra in the early part of the analysis produce effects later after repeated differencing operations described in III. Finally the power series expansion in δP_n tends to fit mean spectra well at the expense of the extremes, which must then be picked up at a later stage of the analysis. The fitting function for the last spectral interval is shown in Figure 5.

Figure 6 is a histogram based on 14,226 spectra. It shows the fraction of these spectra with a given value of $R^i = \left[\sum_{J_\nu=1}^{862} \left\{\delta S^i_{10}(J_\nu)/N(J_\nu)\right\}^2\right]^{1/2} - \sqrt{862}$, where δS^i_{10} is the variability remaining after the best fit using the 9 parameters already described. The quantity R indicates the variability remaining with

respect to that expected due to noise. We see that 56% of the spectra are fitted to within (or better than) the expected noise.

CONCLUSIONS

The results of this study show that measurements in eight moderately wide spectral intervals, plus one high resolution measurement, are adequate to determine spectral variability in the region 400-1600 cm^{-1}, at the signal to noise ratio of the IRIS. From column 5 of table one it is clear that the variability in the first spectral channel is much greater than that in any other interval. The next largest variation, in channel 3, is smaller by a factor of 8. It is significant that channel 1 is an atmospheric window, which sees down through the atmosphere to the surface, or else to the tops of clouds. Surface and cloud top temperatures vary on a smaller spatial scale than other meteorological quantities which may be observed in the IRIS spectral band pass. Therefore, this study suggests that the optimum satellite meteorological sensor in this frequency range is a sounder-scanner. Such an instrument would combine a multi-channel sounder having a moderate field of view with a high spatial resolution scanner in the spectal region 800 to 1000 cm^{-1}, or 800 to 1200 cm^{-1}. The sounder would provide information on atmospheric temperature, water vapor, etc., while the scanner would provide the lower boundary condition such as surface temperature or cloud topography. To date no instrument of this type has been flown, as accurate spatial registration of current sounder data with scanner data has not been accomplished.

For studies of minor constituents of the atmosphere, or atmospheric pollutants, it may be desirable to measure spectral variation in additional spectral intervals. This work indicates that higher signal to noise ratios, or better spectral resolution than IRIS is required in order to obtain information independent from that in the 9 spectral bands listed in Table 1.

REFERENCES

Apostol, T. M., Mathematical Analysis, Addison Wesley, Reading, Massachusetts, 1957, p. 306.

Curran, R. J., Variation of Cloud Emissivity in the Infrared, Conference on Atmospheric Radiation, A.M.S., Fort Collins, Colorado, August 7-9, 1972, p. 103.

Hanel, R. A., Conrath, B. J., Kunde, V. G., Prabhakara, C., Revak, I., Salomonson, V. V., and Wolford, G. , The Nimbus 4 Infrared Spectroscopy Experiment, I. Calibrated Thermal Emission Spectra, J. Geophys. Res., 77, 1972, p. 2629.

Kunde, V. G., and Maguire, W. C., Direct Integration Transmittance Model, 1974, to be published in J. of Quantitative Spectroscopy and Radiative Transfer.

Lawley, D. N. and Maxwell, A. E., Factor Analysis as a Statistical Method, Butterworths, London, 1963, p. 2.

The Nimbus IV Users Guide, The Infrared Interferometer Spectrometer (IRIS) Experiment, Goddard Space Flight Center, NASA Greenbelt, Maryland, 1970, p. 65.

Table 1

Variable	ν^o	ν^f	$\bar{P}$	$\sqrt{(\delta\bar{P}^2)}$	$\sqrt{(\delta\bar{P}^2)}/\bar{P}$	Meteorological Association
1	770.6	981.9	15,100	5,338	0.354	Surface or cloud top temperature
2	632.9	702.4	3,132	480.7	0.153	Temperature profile
3	446.6	605.1	14,326	677.3	0.047	Lower tropospheric humidity
4	991.7	1066.7	2,987	193.2	0.065	Ozone variability
5	706.6	740.0	2,013	50.5	0.025	Temperature profile
6	667.7	670.5	158	11.2	0.071	Temperature profile
7	751.1	823.4	5,812	62.4	0.011	Temperature profile
8	1069.5	1146.0	3,288	95.2	0.029	Desert Surface (reststrahlen)
9	1483.9	1550.6	181	45.4	0.251	Upper tropospheric humidity

FIGURE CAPTIONS

Figure 1. Representative noise equivalent radiance for the IRIS instrument

Figure 2. Zero order fit to IRIS spectra with radiance of 14,300 ergs--cm^{-2} -$ster^{-1}$ -ser^{-1} in the spectral band 771-982 cm^{-1}

Figure 3a-f. One parameter fit to the IRIS spectra using radiance from the 771-982 cm^{-1} window

Figure 4a-f. Fitting functions S_2 through S_9 are plotted at plus one standard deviation values of power in the respective spectral bands defined in Table 1.

Figure 5. The fitting function S_{10} shows substantial variability in the first spectral band as well as magnified effects of instrument noise.

Figure 6. In this histogram the fraction of an ensemble of spectra with a given residual variability is shown as a function of this variability. The variation expected from noise has been subtracted out.

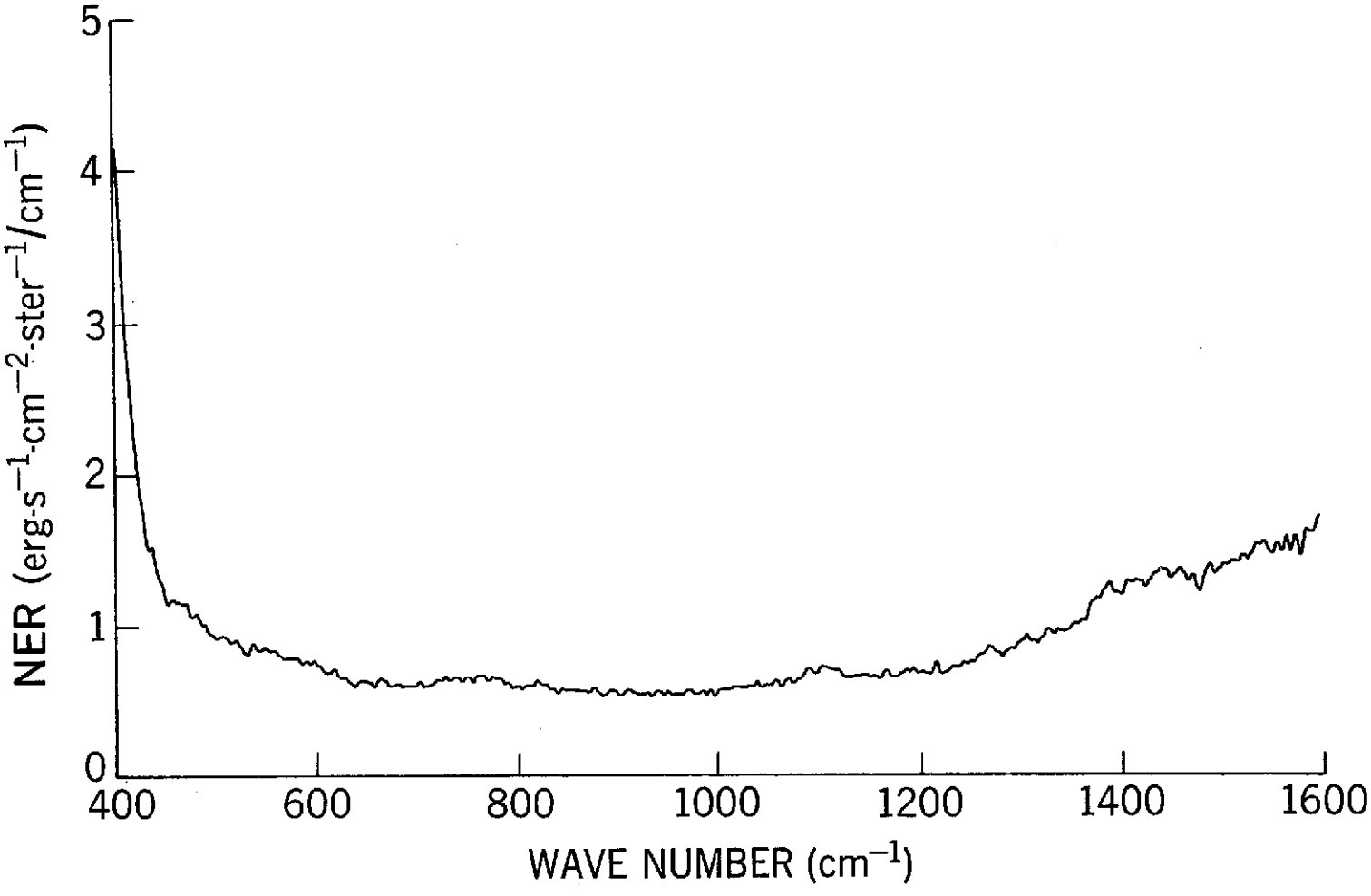

Figure 1. Representative Noise Equivalent Radiance for the IRIS Instrument

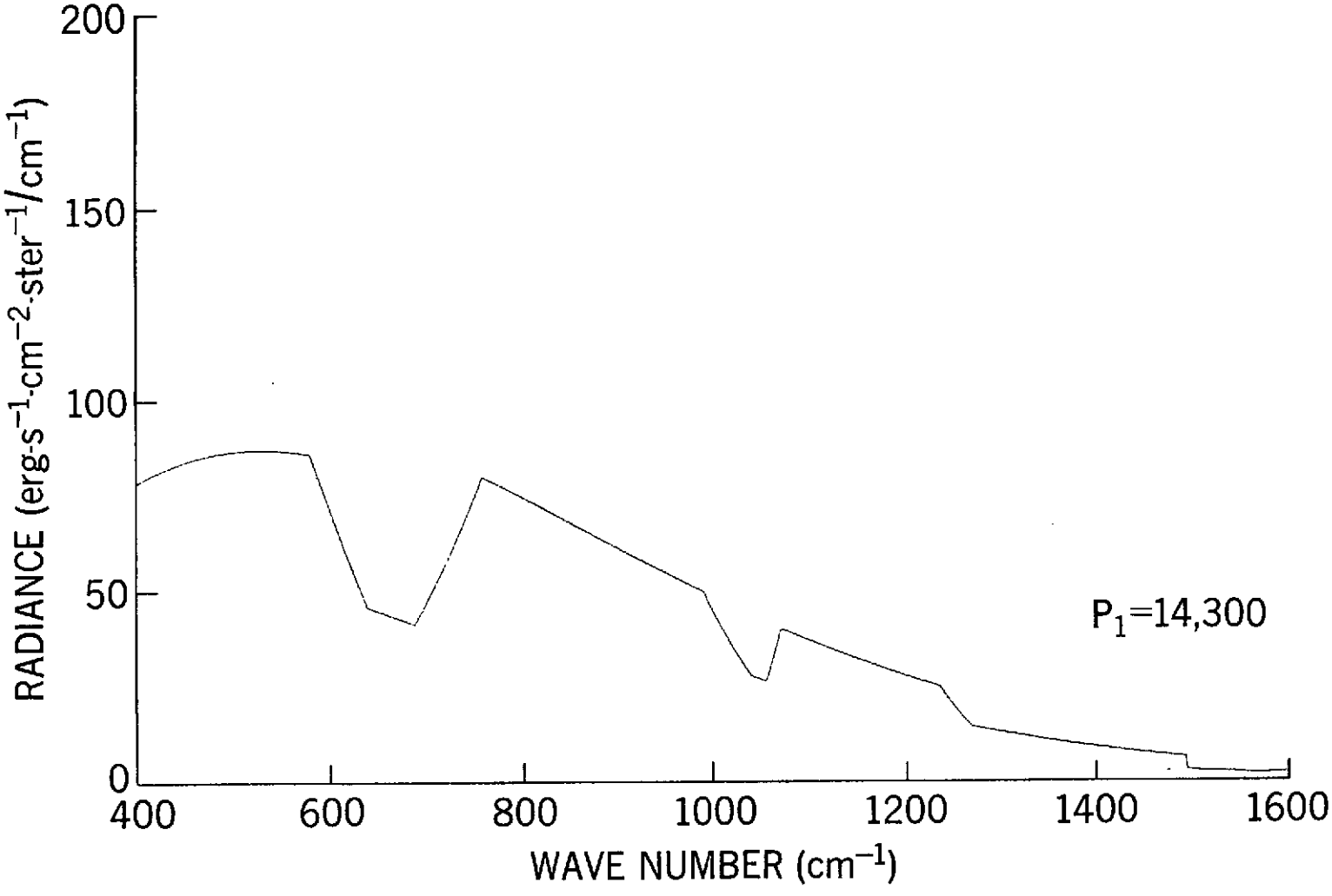

Figure 2. Zero Order Fit to IRIS Spectra with Radiance of 14,300 ergs--cm^{-2} -ster^{-1} -ser^{-1} in the Spectral Band 771-982 cm^{-1}

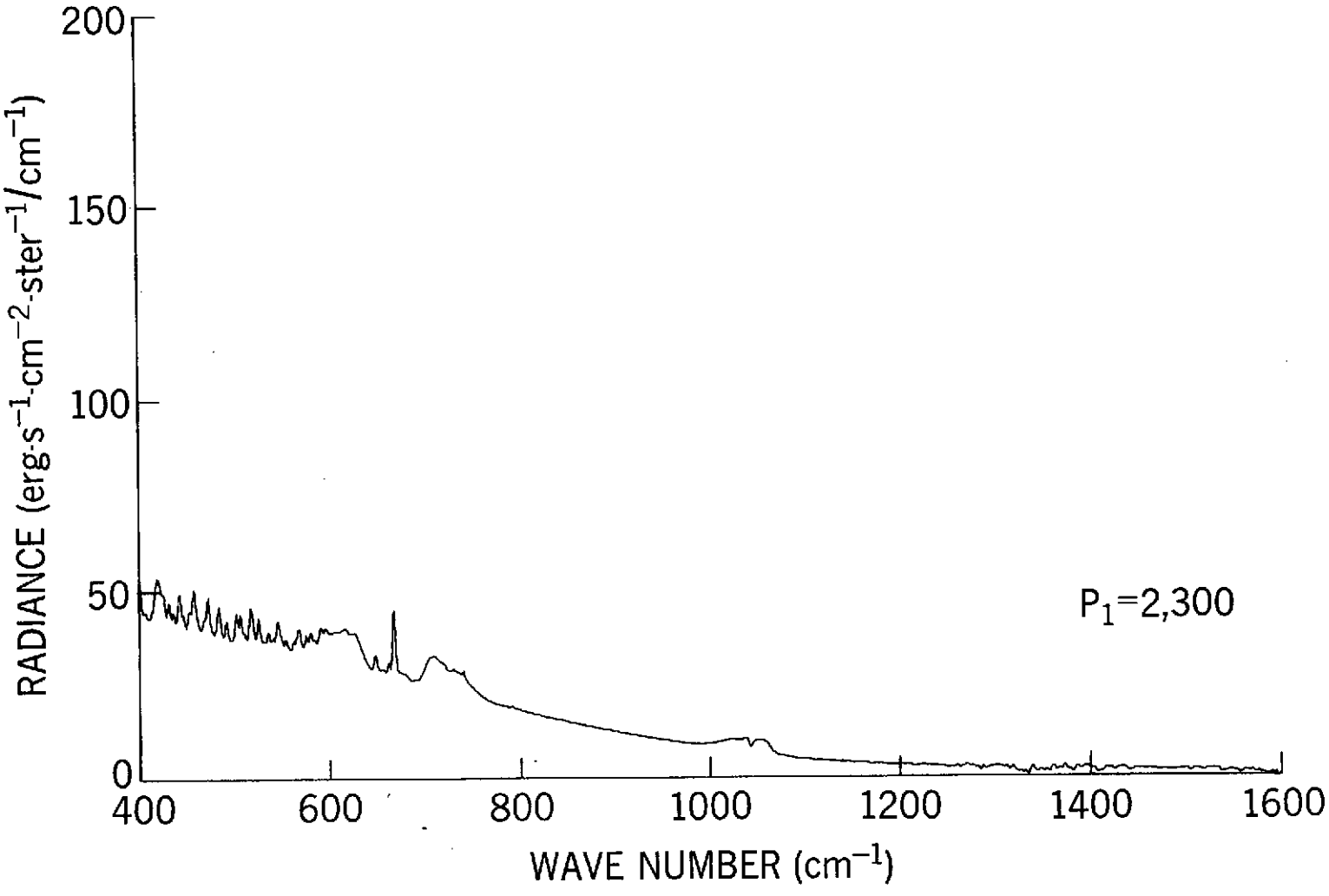

Figure 3a. One Parameter Fit to the IRIS Spectra Using Radiance from the 771-982 cm^{-1} Window

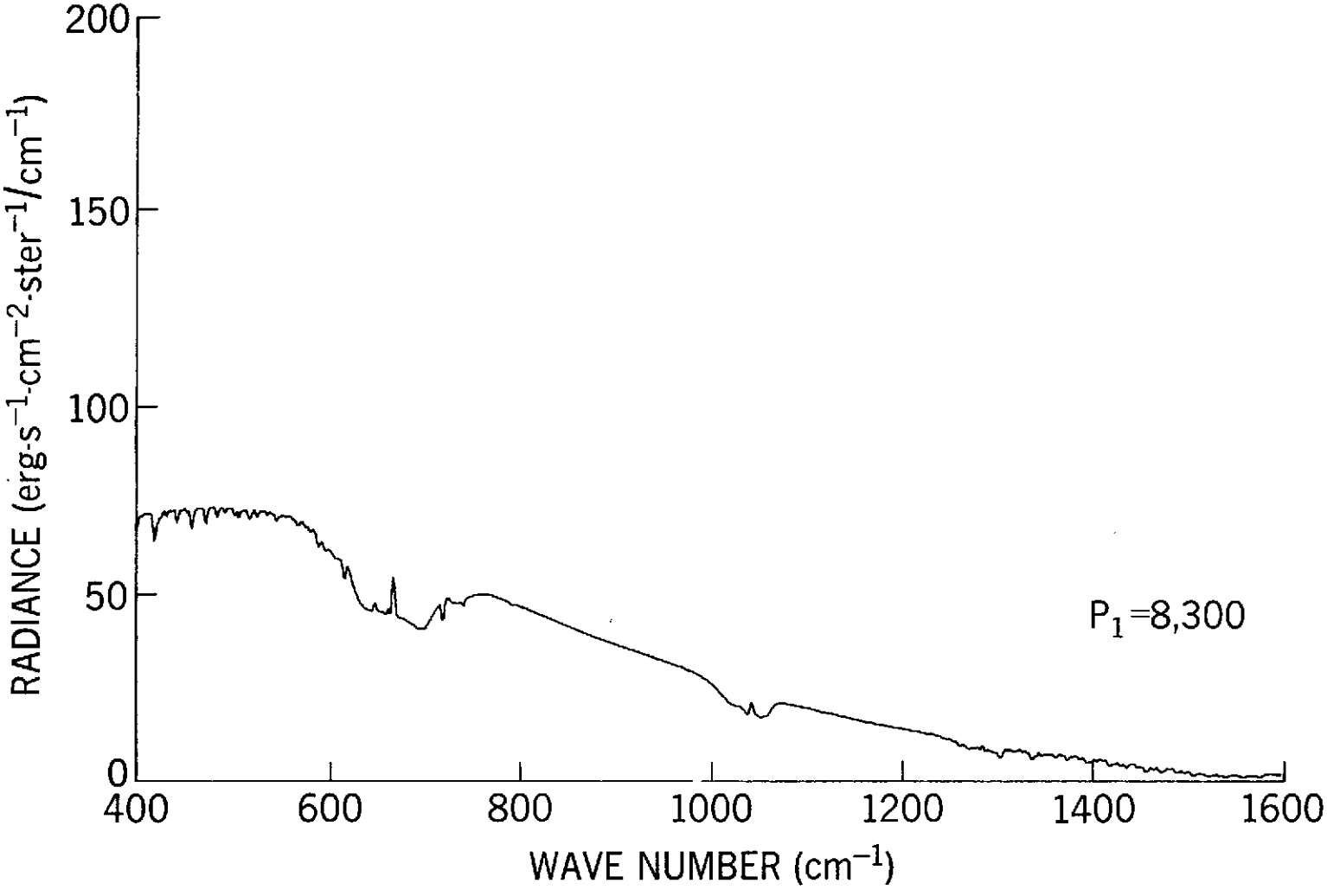
200
150
100
50
0
RADIANCE (erg·s⁻¹·cm⁻²·ster⁻¹/cm⁻¹)
400
600
800
1000
1200
1400
1600
WAVE NUMBER (cm⁻¹)
P1=8,300

Figure 3b.

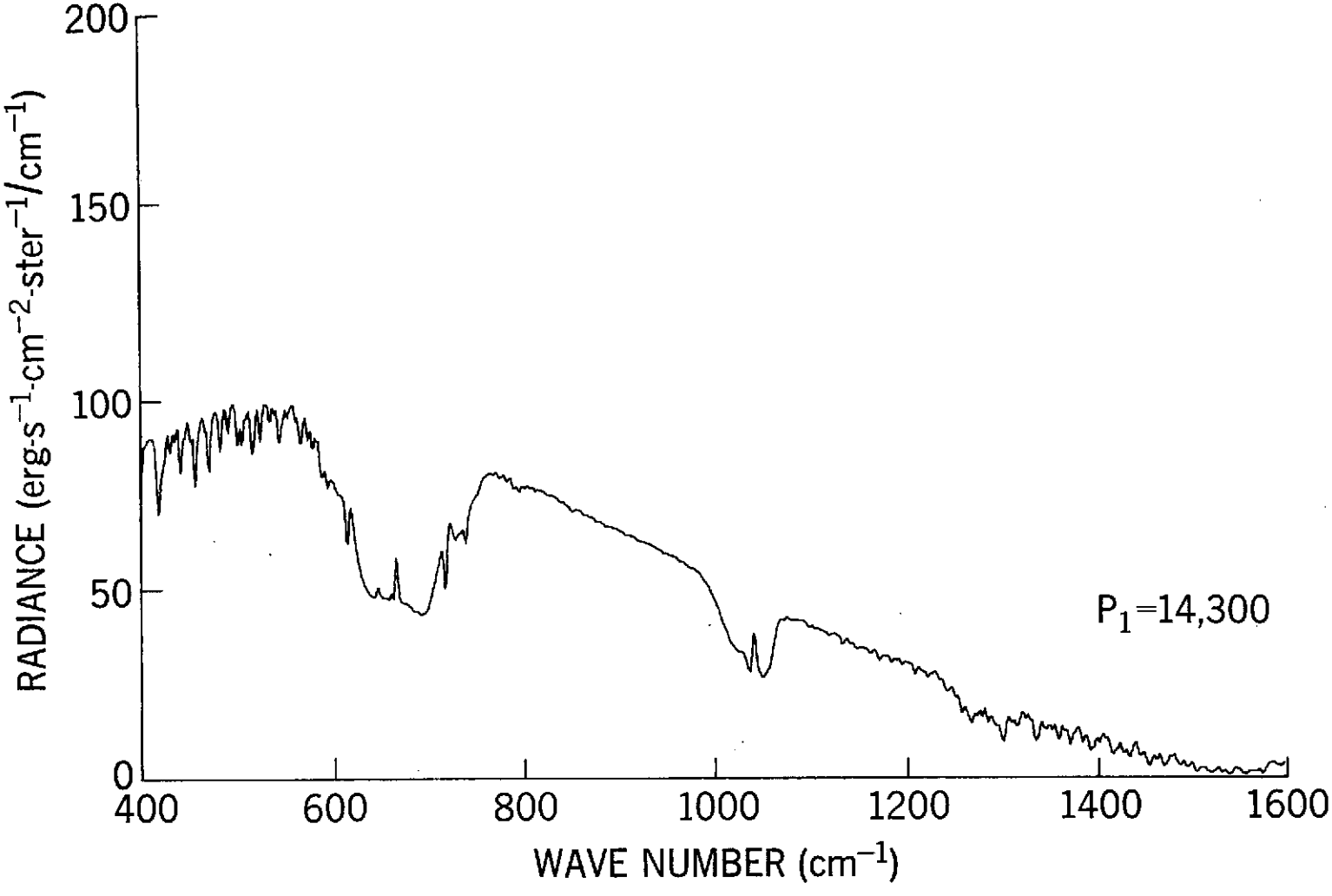
200
150
100
50
0
RADIANCE (erg·s^{-1}·cm^{-2}·ster^{-1}/cm^{-1})
400
600
800
1000
1200
1400
1600
WAVE NUMBER (cm^{-1})
P_1=14,300

Figure 3c.

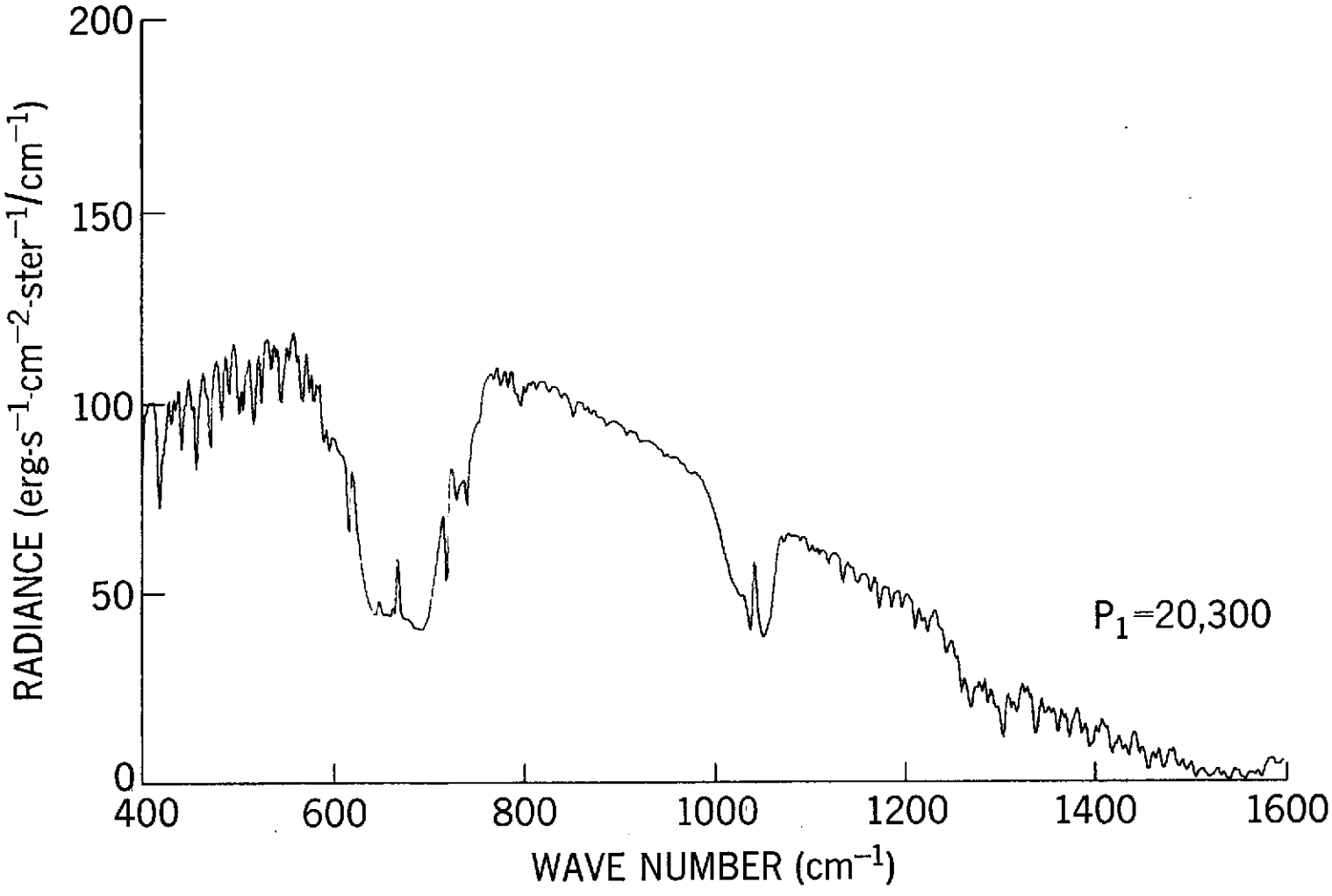
200
150
100
50
0
RADIANCE (erg·s⁻¹-cm⁻²-ster⁻¹/cm⁻¹)
400
600
800
1000
1200
1400
1600
WAVE NUMBER (cm⁻¹)
P1=20,300

Figure 3d.

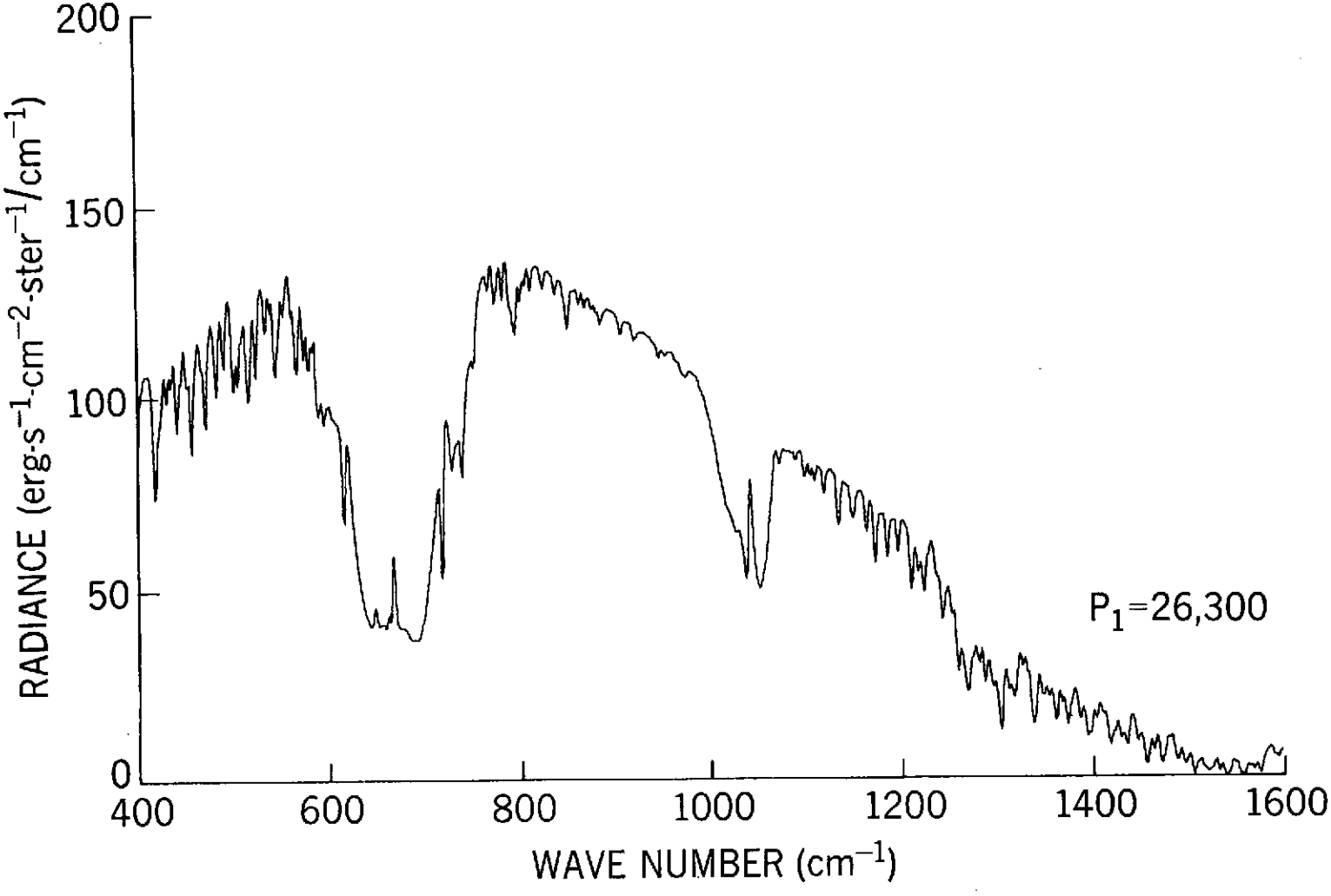
200
150
100
50
0
RADIANCE (erg·s⁻¹-cm⁻²-ster⁻¹/cm⁻¹)
400
600
800
1000
1200
1400
1600
WAVE NUMBER (cm⁻¹)
P1=26,300

Figure 3e.

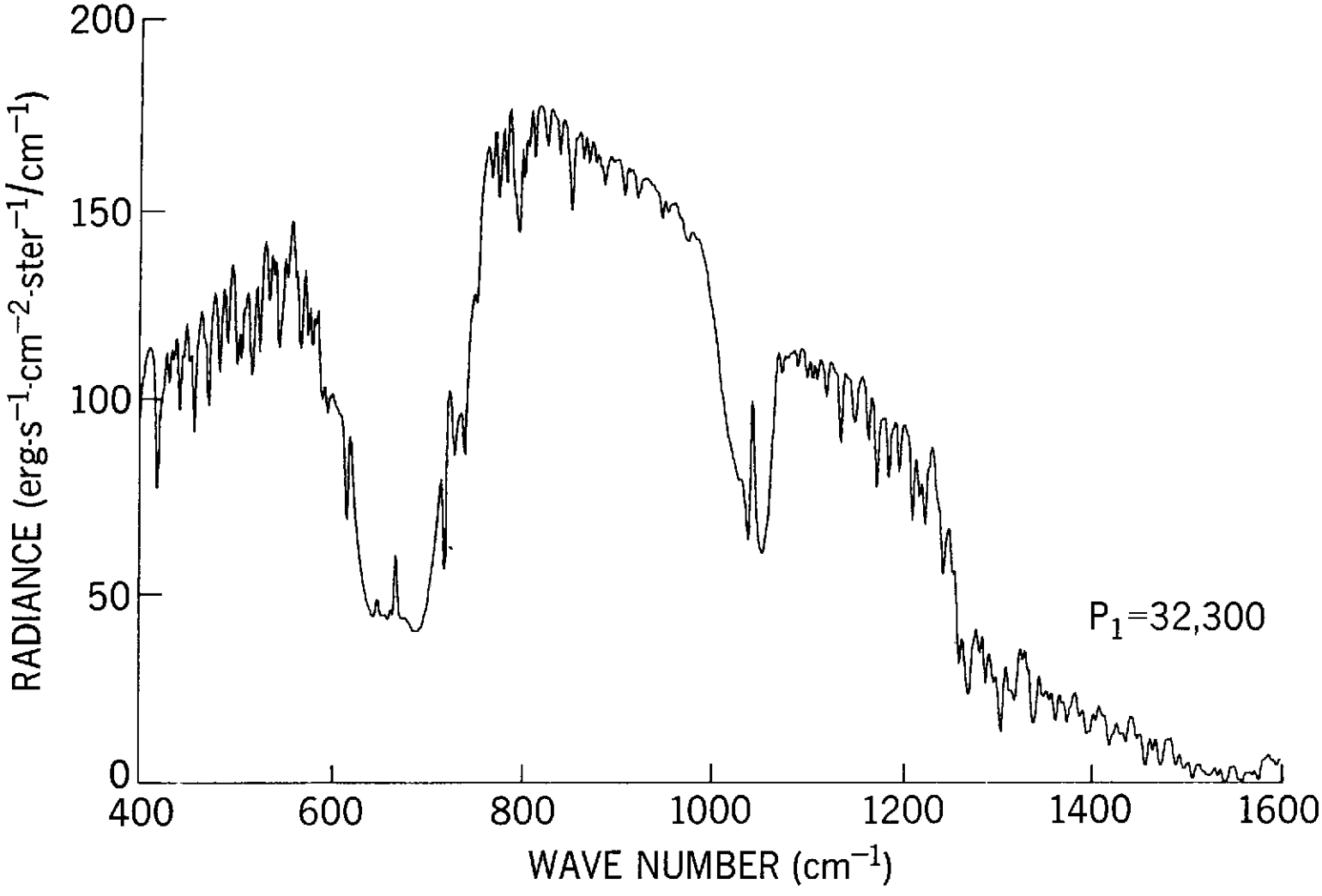
200
150
100
50
0
RADIANCE (erg·s^{-1}·cm^{-2}·ster^{-1}/cm^{-1})
400
600
800
1000
1200
1400
1600
WAVE NUMBER (cm^{-1})
P_1=32,300

Figure 3f.

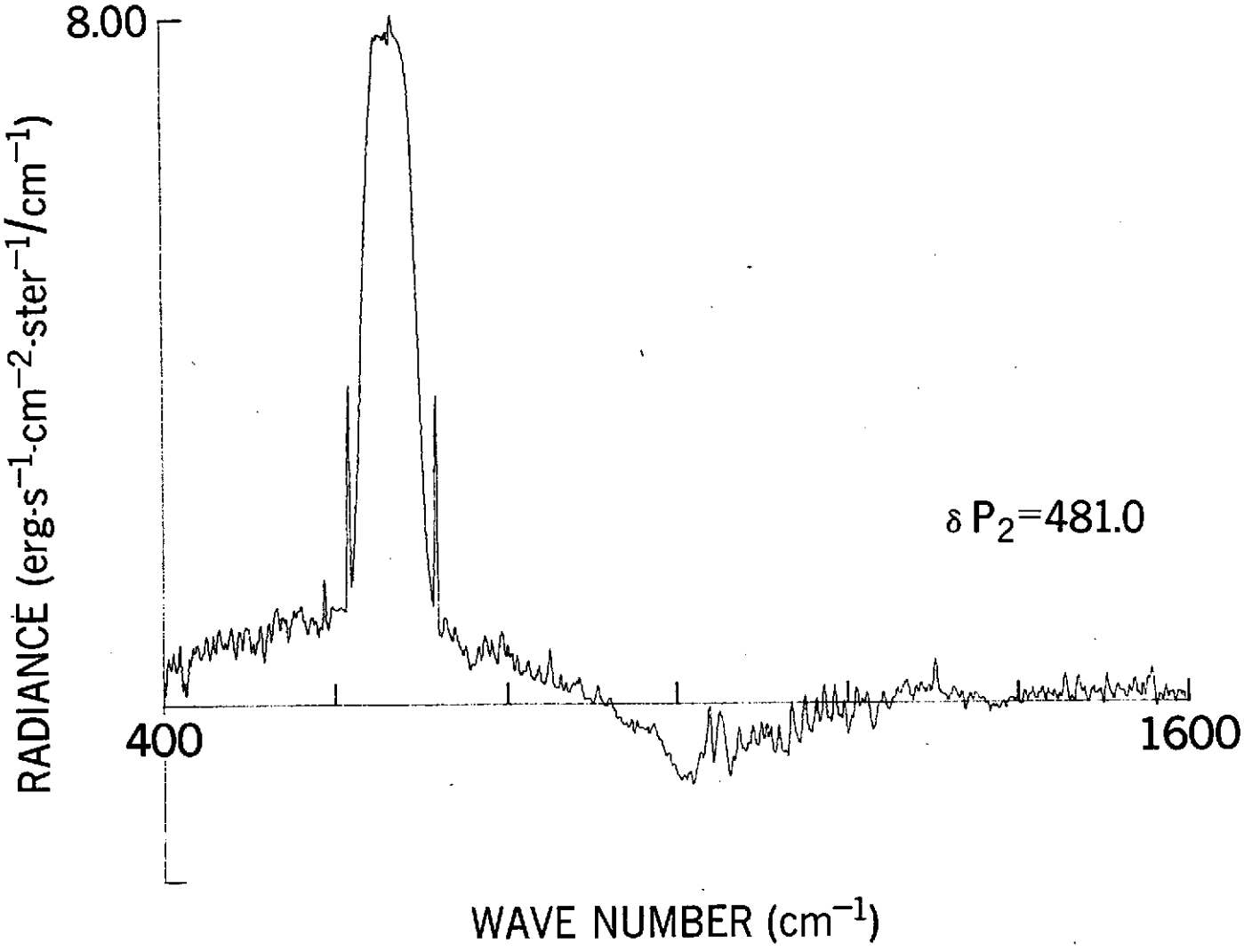

Figure 4a. Fitting functions S_2 through S_9 are plotted at plus one standard deviation values of power in the respective spectral bands defined in Table 1.

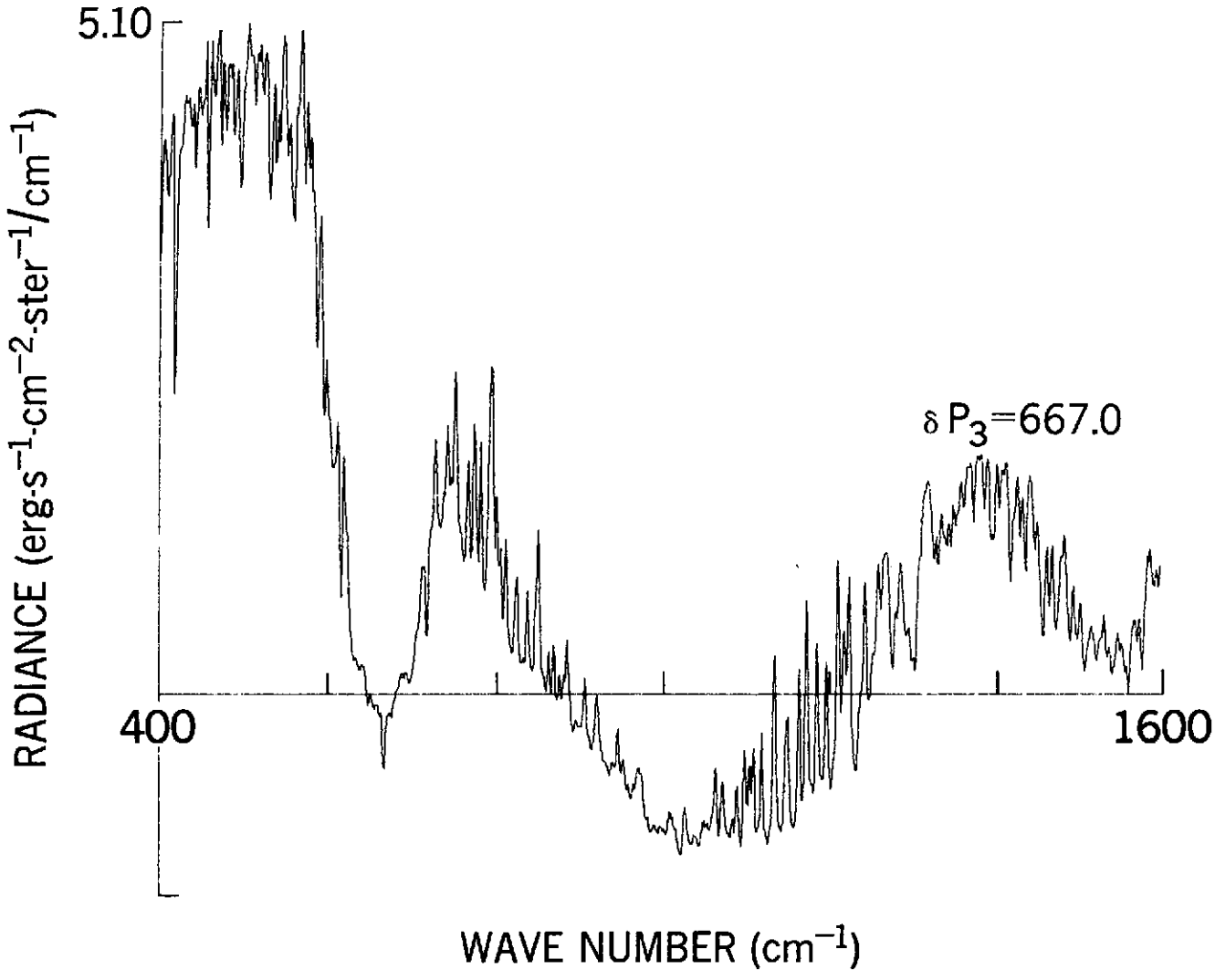
5.10
RADIANCE (erg·s^{-1}·cm^{-2}·ster^{-1}/cm^{-1})
δ P$_3$=667.0
400
1600
WAVE NUMBER (cm^{-1})

Figure 4b.

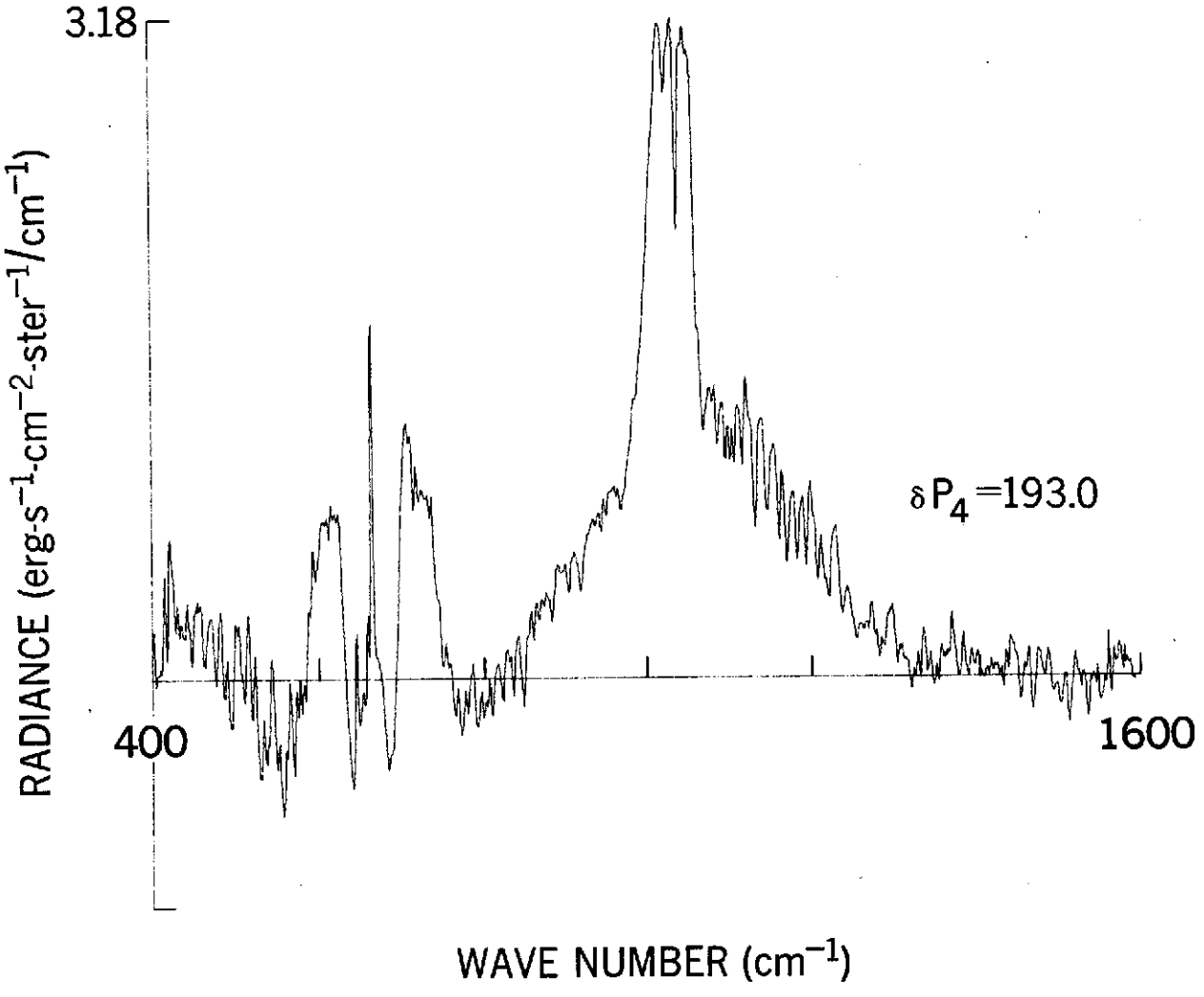
3.18
RADIANCE (erg-s^{-1}-cm^{-2}-ster^{-1}/cm^{-1})
δP_4 =193.0
400
1600
WAVE NUMBER (cm^{-1})

Figure 4c.

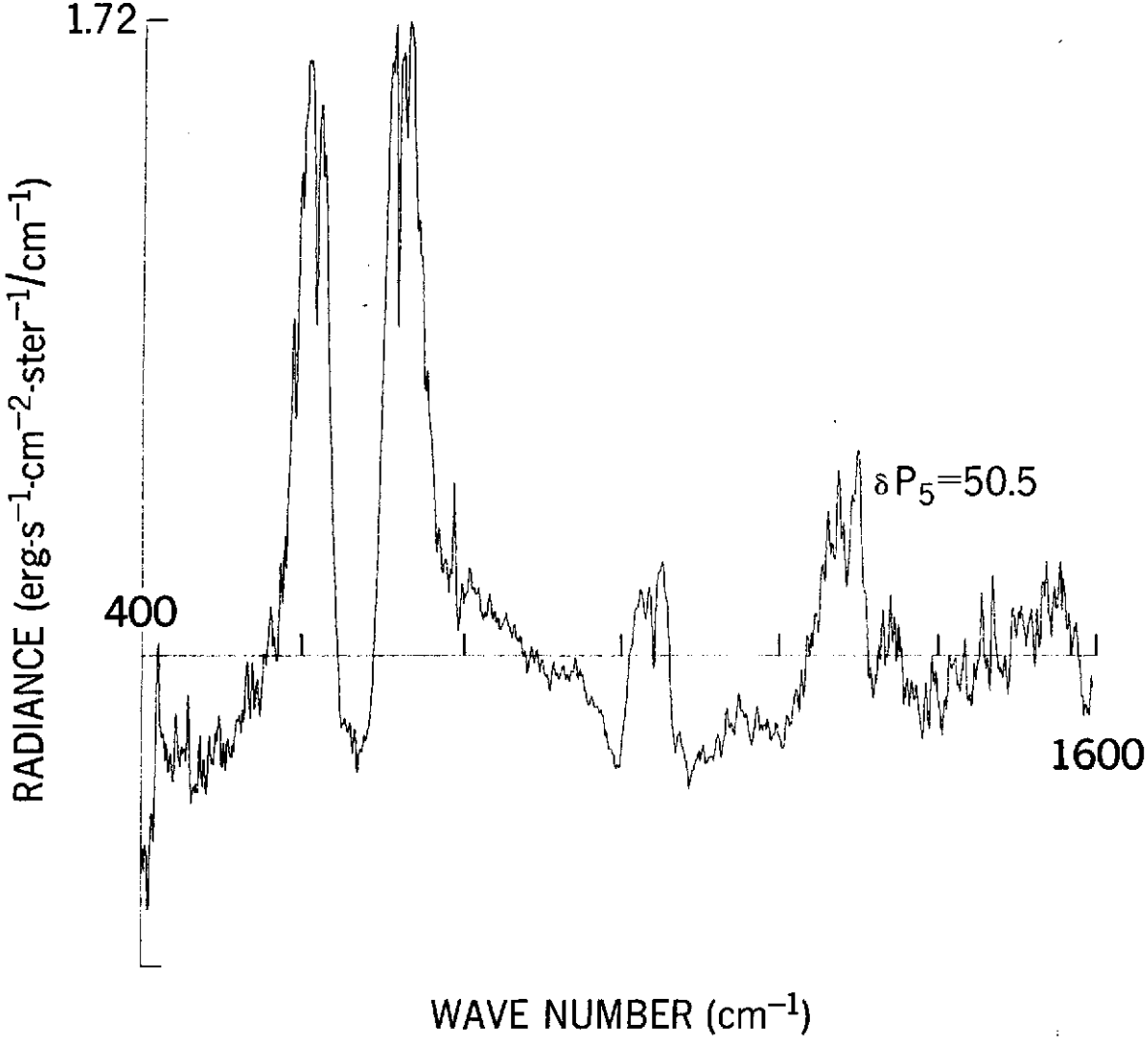
1.72
400
1600
RADIANCE (erg·s^{-1}-cm^{-2}-ster^{-1}/cm^{-1})
WAVE NUMBER (cm^{-1})
δP$_5$=50.5

Figure 4d.

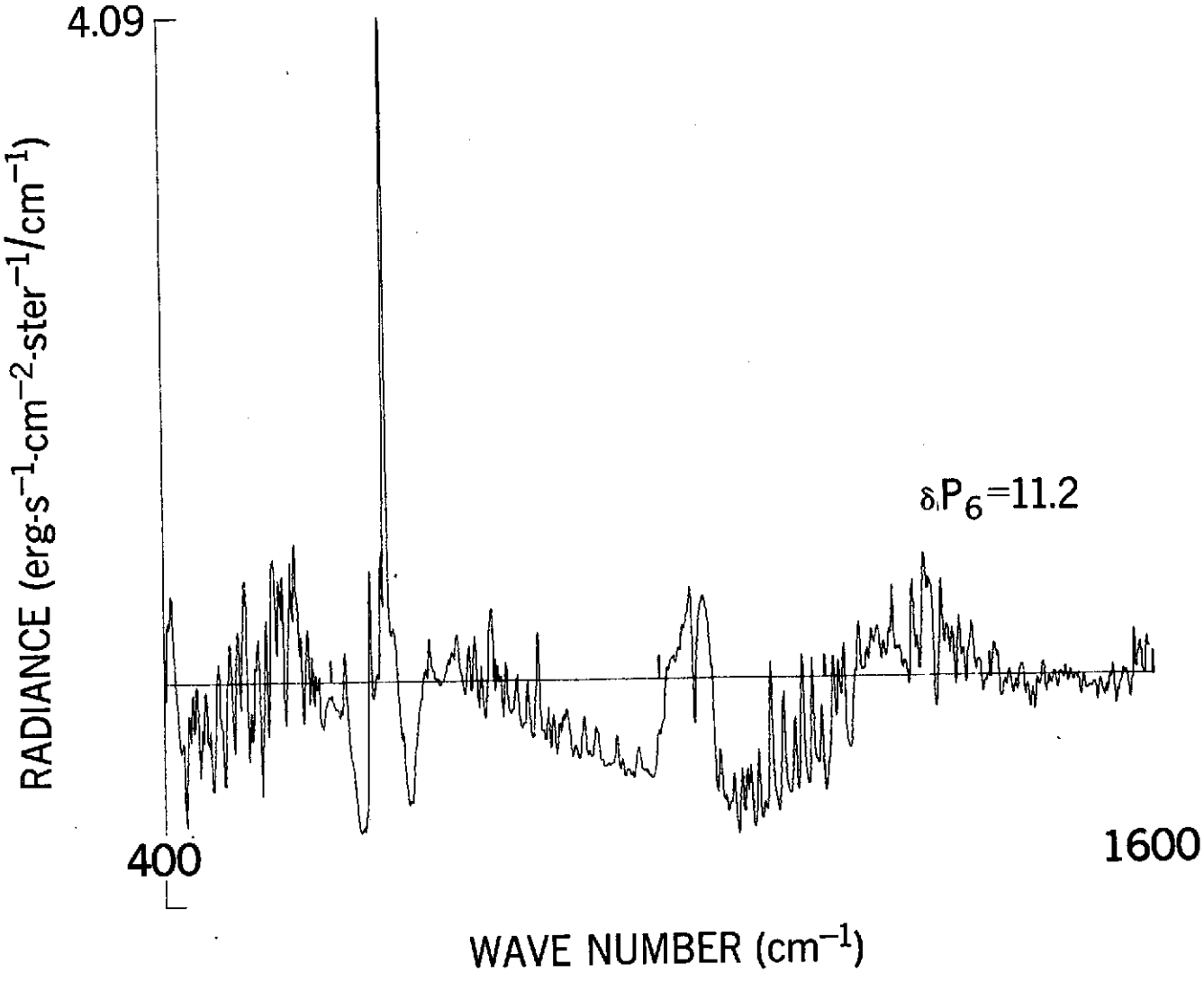
4.09
RADIANCE (erg-s^{-1}-cm^{-2}-ster^{-1}/cm^{-1})
$\delta_i P_6$=11.2
400
1600
WAVE NUMBER (cm^{-1})

Figure 4e.

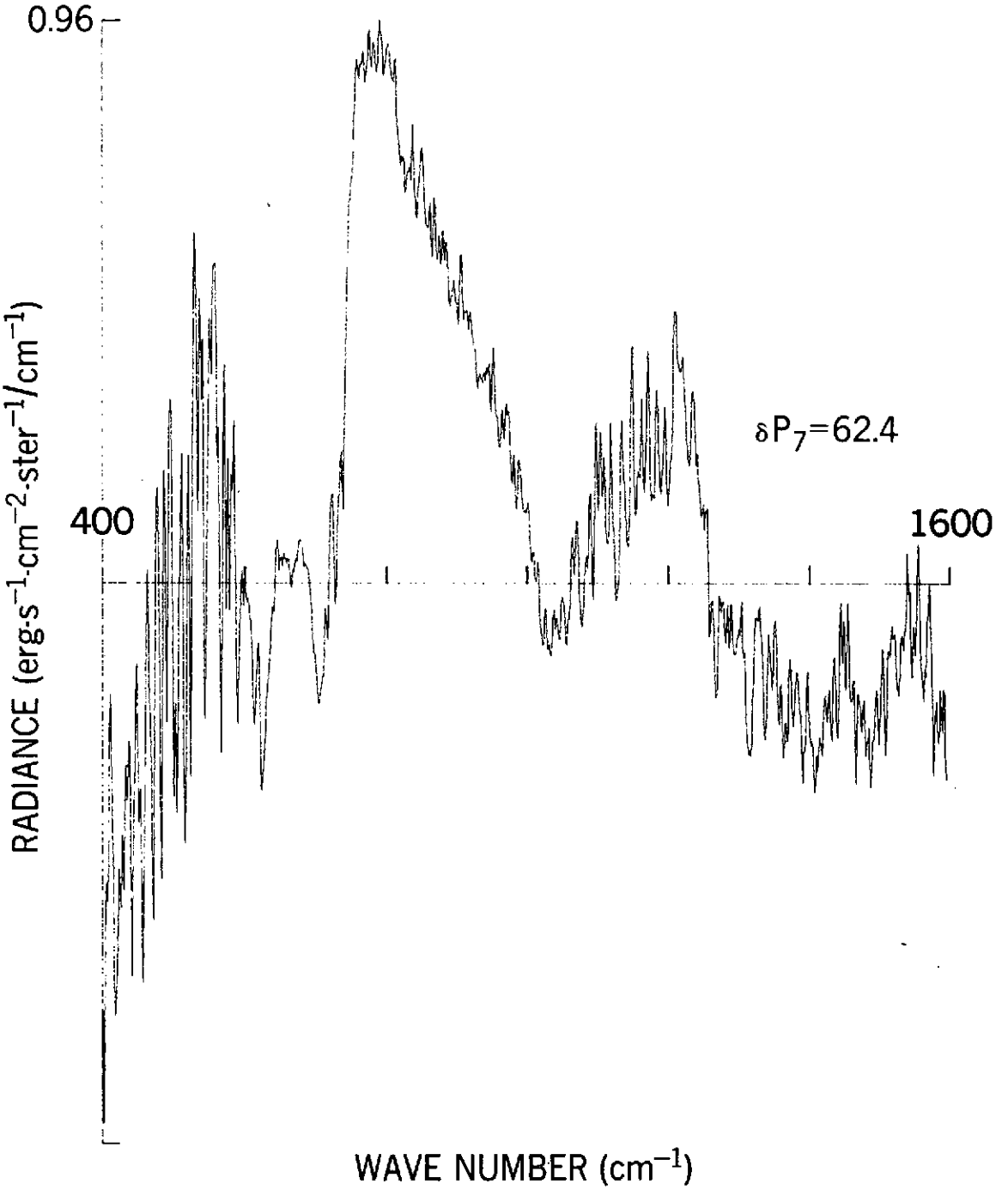
0.96
400
1600
δP_7=62.4
RADIANCE (erg·s^{-1}·cm^{-2}·ster^{-1}/cm^{-1})
WAVE NUMBER (cm^{-1})

Figure 4f.

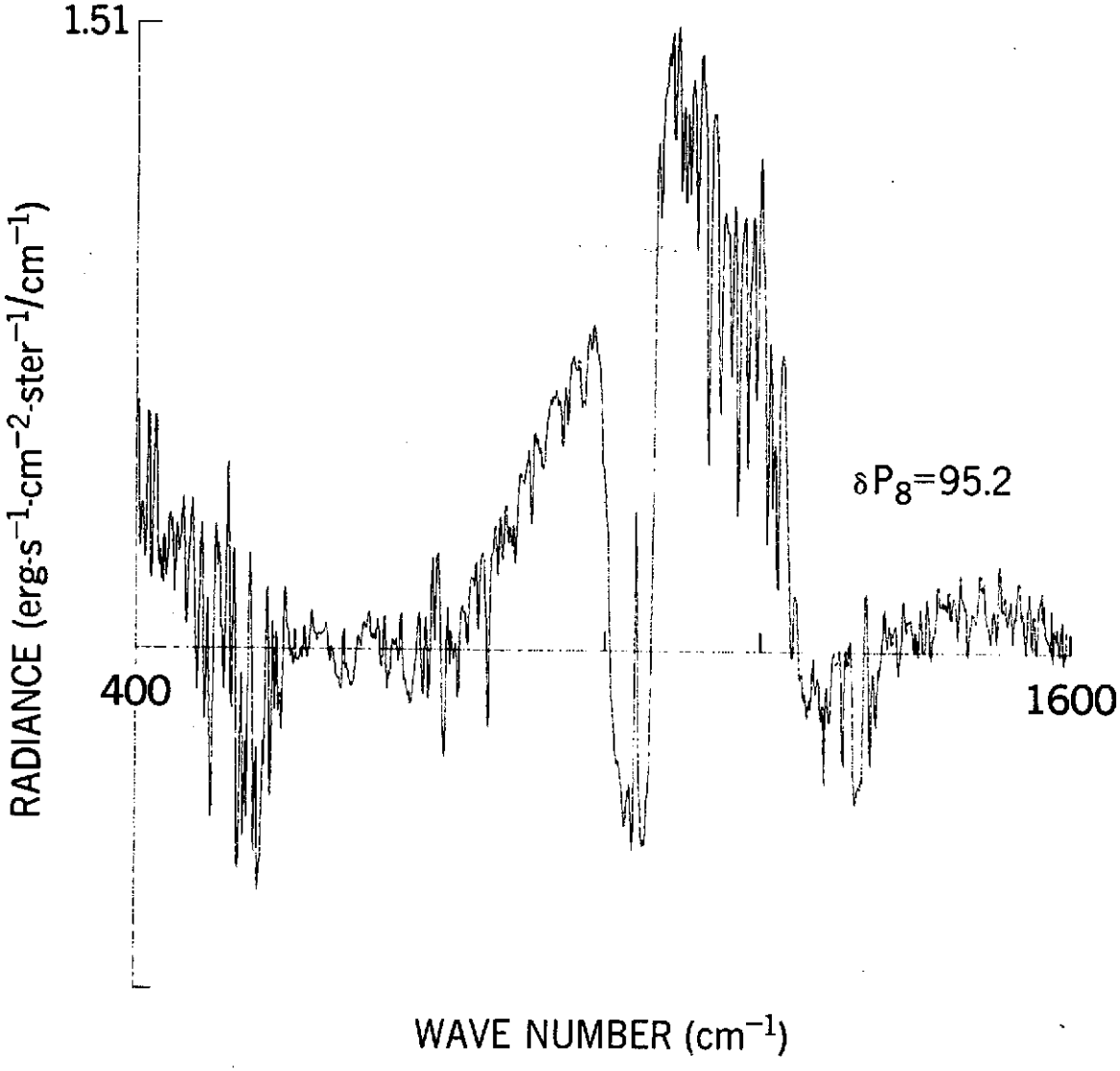
1.51
RADIANCE (erg·s⁻¹·cm⁻²·ster⁻¹/cm⁻¹)
δP8=95.2
400
1600
WAVE NUMBER (cm⁻¹)

Figure 4g.

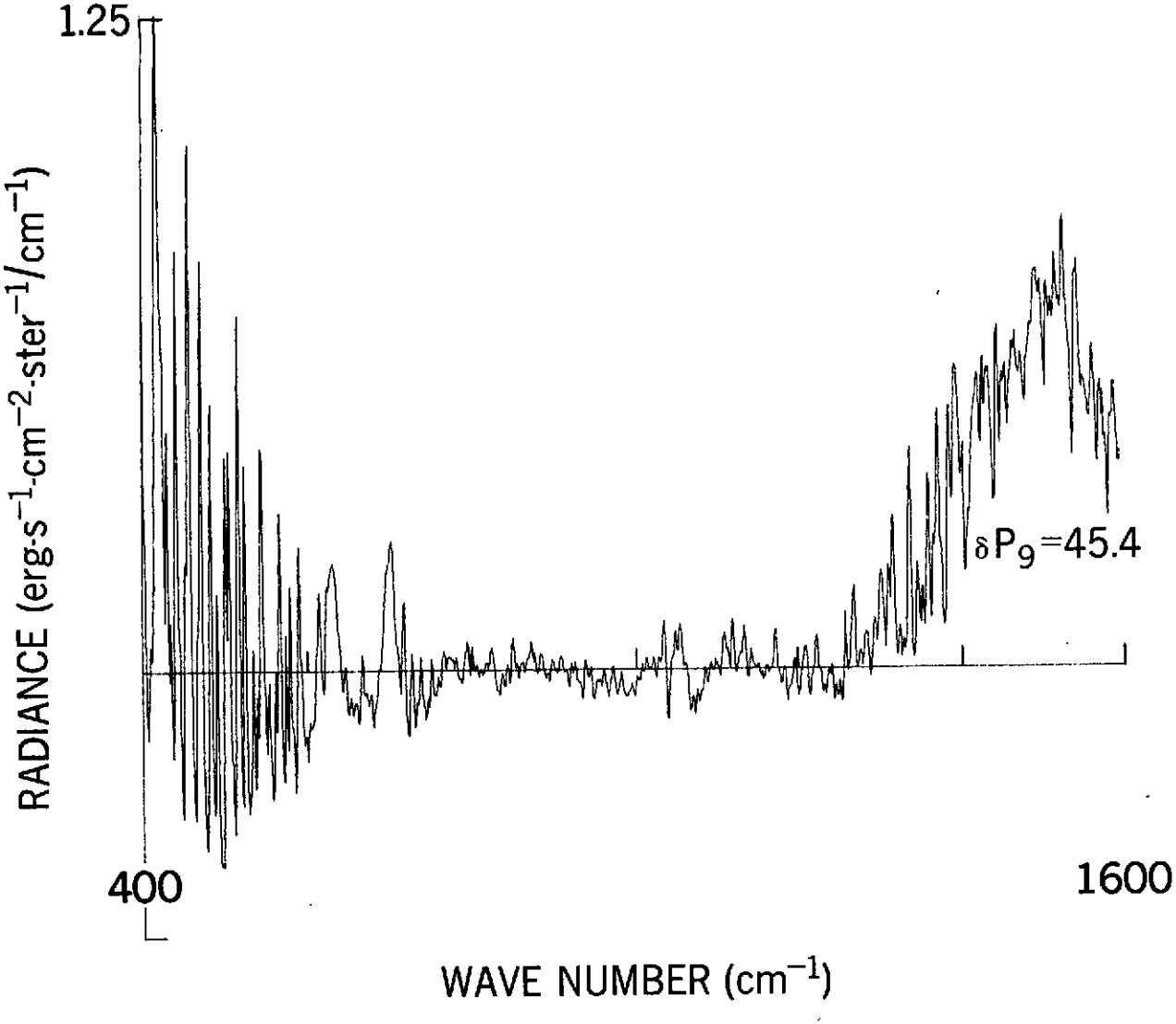
1.25
RADIANCE (erg·s^{-1}-cm^{-2}·ster^{-1}/cm^{-1})
δP$_9$=45.4
400
1600
WAVE NUMBER (cm^{-1})

Figure 4h.

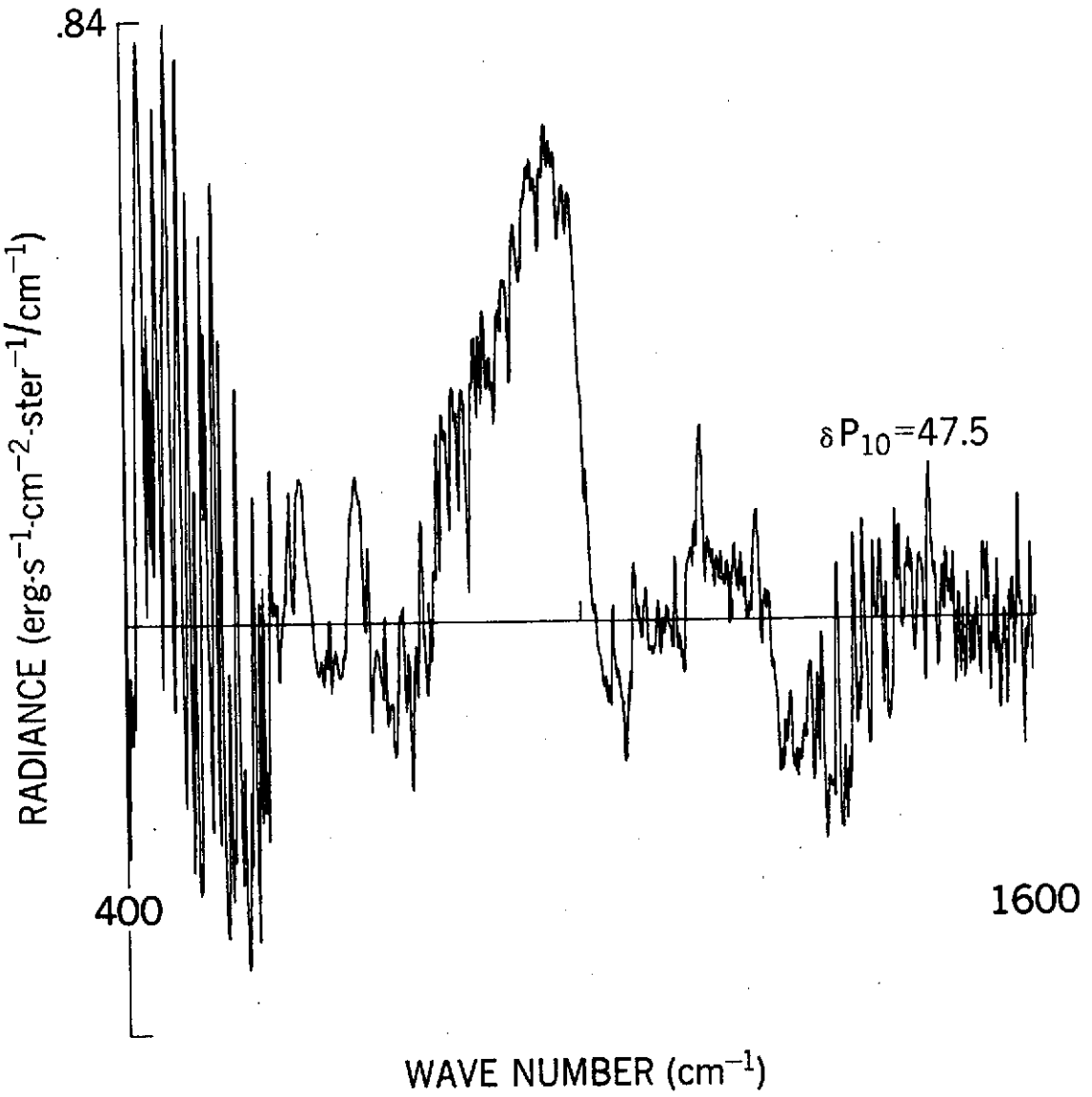

Figure 5. The fitting function S_{10} shows substantial variability in the first spectral band as well as magnified effects of instrument noise.

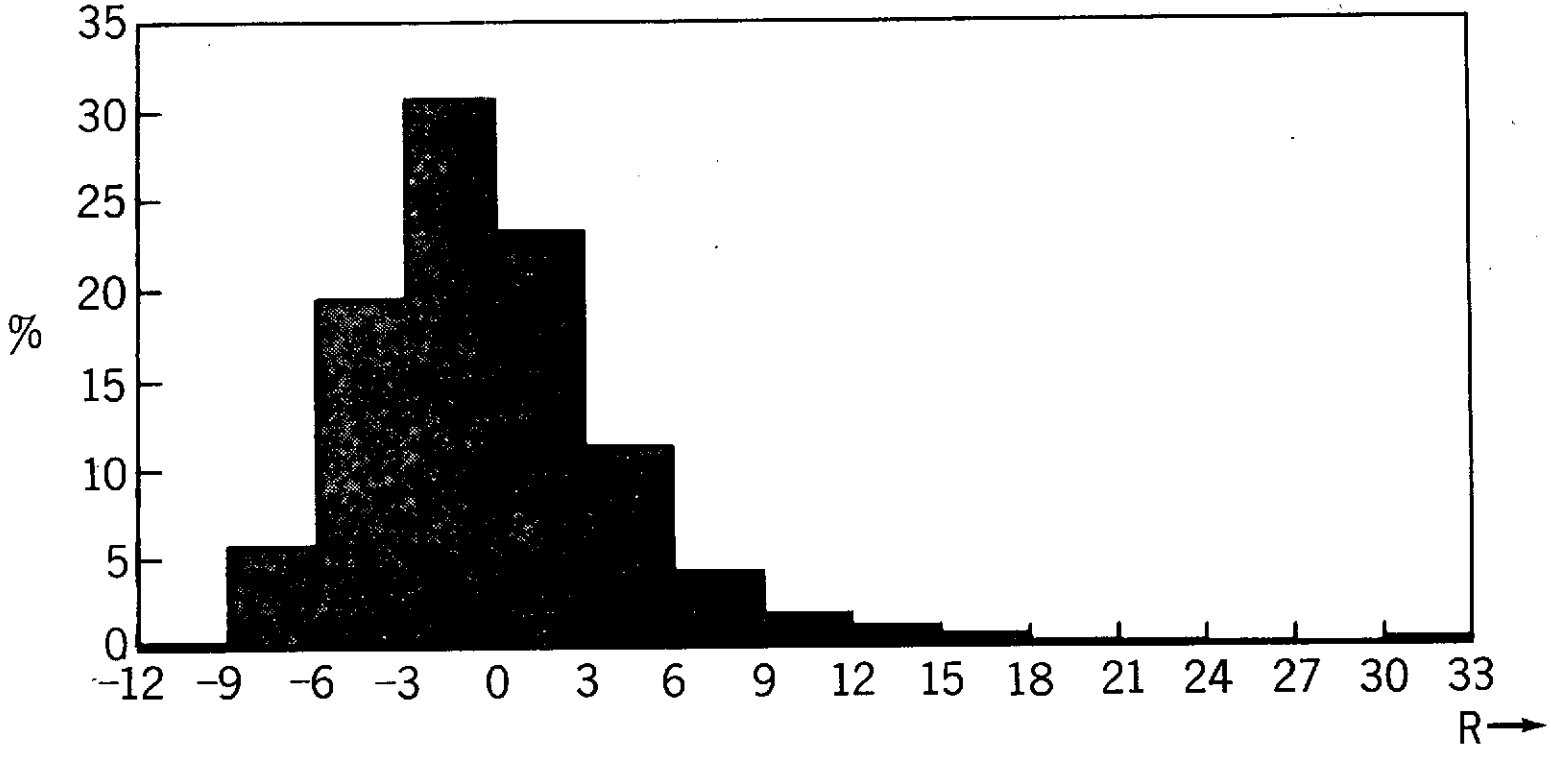

Figure 6. In this histogram the fraction of an ensemble of spectra with a given residual variability is shown as a function of this variability. The variation expected from noise has been subtracted out.